Supplementary Material for "Static adhesion hysteresis in elastic structures"

Edvin Memet[1], Feodor Hilitski[2], Zvonimir Dogic[2,3] and L. Mahadevan[1,4]
[1]*Department of Physics, Harvard University, Cambridge, Massachusetts 02138, USA*
[2]*Department of Physics, Brandeis University, Waltham, Massachusetts 02453, USA*
[3]*Department of Physics, University of California, Santa Barbara, California 93106, USA*
[4]*School of Engineering and Applied Sciences, Department of Organismic and Evolutionary Biology, Harvard University, Cambridge, Massachusetts 02138, USA*
(Dated: January 28, 2021)

CONTENTS

S.1. SIMULATION DETAILS

Numerical simulations for both the flat substrate (e.g. graphene) and curved substrate (e.g. microtubules) conditions were carried out using Espresso (v.3.3.1), a molecular dynamics software [1, 2]. The only difference between the two cases lies in the boundary conditions: in the first case one of the filaments is fixed to a flat surface while in the second case the filament is attached to a bead of size $b = 0.5\mu$m at either end (Fig. S1).

Filaments were coarse grained as a one-dimensional collection of point masses connected by springs of very large stifness k (modeling inextensibility). Triplets of neighboring particles encode a bending interaction that depends on the angle ϕ determined by the triplet. Explicitly,

$$V_{\text{stretch}} = \frac{1}{2}k\left(\Delta l' - \Delta l\right)^2, \tag{S.1}$$

$$V_{\text{bend}} = \frac{1}{2}\frac{B}{\Delta l}\left(\phi - \phi_0\right)^2, \tag{S.2}$$

where $\phi_0 = \pi$. Figure S1 illustrates these bending and stretching interactions in the case of a single filament, with optical bead boundary conditions. The second filament (not pictured) exhibits the same kind of stretching and bending interactions along its length but also interacts adhesively with the first one (as shown in Fig. 1A and Fig. 3A of the main text). The adhesive interaction is modeled by breakable Hookean springs of stiffness K, rest length y_0 and cutoff $y_0 + y_c$.

$$V_{\text{adhesion}} = \begin{cases} \frac{1}{2}K\left(y - y_0\right)^2, & y < y_0 + y_c \\ \frac{1}{2}K\left(y_c\right)^2, & y \geq y_0 + y_c \end{cases} \tag{S.3}$$

In the case of the optical bead boundary condition, the beads are represented as masses connected to their attachment points by springs of stiffness k_b and rest length equal to the radius of the bead b. The optical beads are enforced to remain normal to the filament at the attachment point by defining a bending energy $V_{\text{bend,bead}} = \frac{1}{2}\kappa_b\left(\phi_b - \pi/2\right)^2$ with a sufficiently large κ_b and rest angle $\pi/2$ for the triplet consisting of the bead, its attachment point, and a neighboring mass (Fig. S1, left inset).

Simulations were conducted quasistatically, by incrementally displacing the system then allowing it to relax for a sufficiently long time, and under high damping conditions (low Reynolds number). Relaxation is allowed to run for an arbitrarily large number of timesteps, until the kinetic energy of the system drops below a very small threshold. The values of the damping coefficient and of the integration time step are chosen to be small enough to belong in the overdamped, numerically stable regime, while being mindful of keeping the runtime reasonably fast.

In the displacement controlled case of the flat-substrate simulations, we increase the vertical coordinate of the free end by some fixed amount in a displacement-controlled manner, without applying any horizontal force or displacement. In the ensuing relaxation phase, we allow the system to relax to equilibrium with the constraint of keeping the vertical coordinate of the free end fixed (while the horizontal coordinate is allowed to change). In the displacement controlled case of the curved-substrate simulations, we displace one optical bead by some fixed (small) horizontal amount and then allow the system to relax to equilibrium. The second bead is kept fixed throughout.

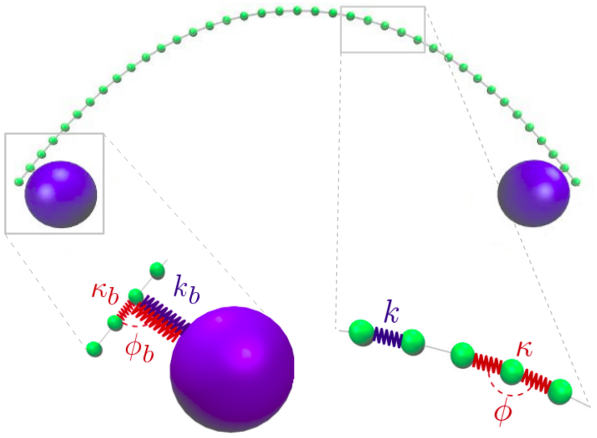

FIG. S1. Schematic of discrete model of a single filament with optical bead boundary conditions (second filament not shown). Green particles discretize the flagellum while blue particles represent the optical beads. The left bead remains fixed, while the right one is incrementally displaced towards or away, which can cause the second filament to peel off or readhere to the first filament. Right inset: closeup of a region of the filament, showing that neighboring masses are connected by linear springs of stiffness k which give rise to a stretching energy according to Eq. S1. In addition, each triplet of neighbors determines an angle ϕ which dictates the bending energy of the unit (Eq. S2). Left inset: closeup of the region where the bead connects to the flagellum. The bead particle is connected to a single particle of the flagellum by a very stiff spring k_b of stress-free length b corresponding to the radius of the optical bead. In addition, there is a bending interaction with angle ϕ_b and stiffness κ_b, aimed at keeping the bead perpendicular to the attachment point. Figure adapted from [3].

S.2. ENERGY LOSS AND HYSTERESIS SCALING

In the case of fraying from a flat substrate, the net energy loss due to a single bond breaking is $\delta E = \delta E_b + \delta E_s < 0$, where δE_b and δE_s are the bending and adhesion energies lost after a bond breaks. Figure S2A shows the relation between the three energies. While δE_b and δE_s both scale as the energy of a single adhesion-modelling spring ($K\, y_c^2$), the scaling of the net energy loss per bond broken (or re-formed) contains an extra factor of $\Delta l/l_H$: $\delta E \sim K y_c^2 \times (\Delta l/l_H) \sim E_b^0 \times (\Delta l/l_H)^2$ (where $E_b^0 \equiv B\kappa_c^2 l_H$ is the natural scale for bending energy). Consequently, the scaled net energy loss $\delta e \equiv \delta E/E_b^0$ scales as $(\Delta l/l_H)^2$:

$$\delta e \sim (\Delta l/l_H)^2 \sim \sqrt{\frac{K}{B}\left(\frac{L}{n}\right)^3}. \tag{S.4}$$

Figure S2B tests the above scaling of δe with n, confirming that the exponent of n is approximately -3/2. Since scaled hysteresis size equals the total energy lost $n\,\delta e$ across all n individual bond breakage events, Eq. (S.4) provides a recipe for predicting and controlling hysteresis. For instance, hysteresis increases with increasing strength K of the adhesive interactions as well as with decreasing bending rigidity B of the filaments, but remains constant as long as the ratio K/B does not change.

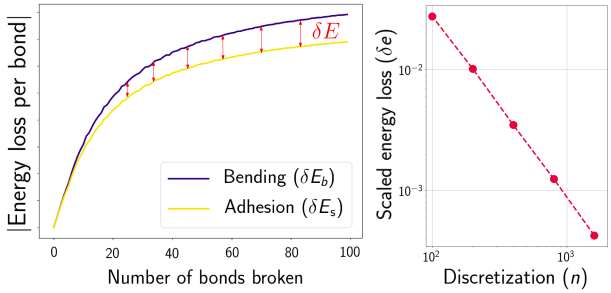

FIG. S2. (A) Absolute values of the filament's bending and adhesion energy changes at bond breakage events (blue and yellow, respectively) as a function of the number of bonds broken. The difference between the two curves represents the net energy loss δE. Parameters: $L = 16\,\mu$m, $B = 22\,pN\,\mu$m^2, $K = 40\,pN/\mu$m, $n = 400$, $y_0 = 5\,$nm, $y_c = 10\,$nm for the case of fraying from a flat substrate. (B) Log-log plot of scaled energy loss δe versus the number of adhesive bonds n, which varies from $n = 70$ to $n = 1600$. All the other parameters are the same as in panel A. Because scaled energy loss δe changes with strain, as in Fig. S2A, the values used for δe in this plot are all taken at the same value of strain.

For the more general case in which both filaments are allowed to bend, as in the microtubule fraying experiments, the same general arguments hold, though the specific functional dependence of scaled energy loss δe changes, since there are now *two* natural energy scales: $K y_c^2 \times (\Delta l/l_H)$ and B/L (see main text). Expressed in terms of the invariant adhesion energy per unit length J rather than in terms of the adhesive spring stiffness K, the scaled energy loss summer over all bonds is:

$$n\,\delta e \sim \frac{L^3}{n\, y_c^{1/2}}\left(\frac{J}{B}\right)^{5/4}. \tag{S.5}$$

This equation suggests that in order to increase hysteresis, we could, for instance, design stronger adhesive interactions, softer filaments, or increase the length of the filaments. We note that some effects are not captured by the above equation, as hysteresis size will also depend nontrivially on the length L_2 of the shorter filament as well as on the maximum strain. Figure S3A illustrates this through data from two simulations in which all conditions are identical except for the length L_2 of the second filament. When $L_2 = 0.7L_1$, the force starts out higher (blue curve) than when $L_2^{'} = 0.6L_1$ (red dashed curve), but once it frays sufficiently, it collapses onto the curve corresponding to $L_2^{'} = 0.6L_1$. Thus, when the other parameters are identical, a larger L_2 produces a larger hysteresis, provided that the maximum strain also stays the same.

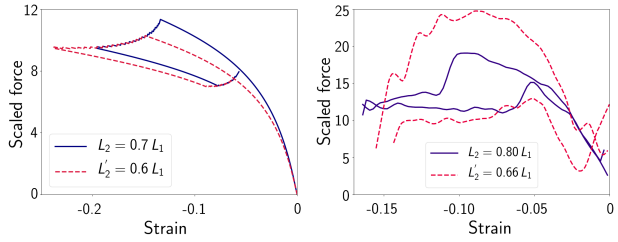

FIG. S3. (A) Scaled force versus strain for simulations in which the length of the shorter filament is varied from $L' = 0.7L$ (blue) to $L' = 0.6L$ (red, dashed). Parameters: $L = 8\,\mu$m, $B = 22\,pN\,\mu$m^2, $K = 400\,pN/\mu$m, $n = 100$, $y_0 = 5$ nm, $y_c = 10$ nm. (B) Experimental data from two distinct experiments in which the length L of the longer microtubules is similar while the length of the shorter microtubules is different (0.8 and 0.66 of L, respectively). Contrary to what we expect based on simulations (panel A) and intuition, the hysteresis size is significantly larger when the second microtubule is shorter. This suggests that experimental data is very noisy, with significant variations in factors that cannot be controlled precisely, such as the stiffness of the microtubules and the strength of the depletion interaction.

To test our predictions for hysteresis size, we examine our data on microtubule fraying experiments. Since Eq. (S.5) does not account for the effect of L_2 on hysteresis size, we are limited to comparing data sets with either equal ratios of filament lengths L_2/L_1 or with equal conditions but different lengths L_2. A comparison of the latter kind (equal L_1; B and J not measured) is shown in Fig. S3B. Surprisingly, the rule that hysteresis decreases when the second filament is shorter is not satisfied in this case, possibly indicating large variations in the bending rigidity B and/or adhesion energy J. In fact, we know it is improper to characterize microtubules by a single bending rigidity as we might do with simple Euler-Bernoulli beams; as anisotropic hollow shells, they exhibit non-classical behavior associated with cross-sectional softening and the subsequent approach to a force plateau and need at least two parameters to characterize their degrees of freedom – circumferential bending and shearing [3]. In the absence of precisely knowing the MT mechanical parameters and adhesion energy in our experiments, it is difficult to experimentally verify our model's prediction on hysteresis scaling.

S.3. BRIDGING THE DISCRETE AND CONTINUUM LIMITS

Our model is practically identical to the model proposed by Thomson et al. [4] in the context of lattice trappings of fracture cracks. In that work, however, the authors were not able to bridge the discrete and continuum limits, noting that "the continuum prediction of a unique equilibrium stress should break down when the discrete nature of the lattice is considered." Equivalently, in our problem, this would be analogous to hysteresis vanishing when a discrete system is brought to the continuum limit. In this manuscript we showed that using a specific, unique, parameter scaling resolves this problem, bridging the discrete and continuum limits and thus reconciling the two pictures. Conversely, a more "intuitive" way of scaling parameters ($K \sim 1/n$) is wrong, leading precisely to the vanishing of hysteresis as $n \to \infty$.

Concretely, if we are simulating a continuum system, for example, we may know its adhesion energy per unit length $J = nKy_c^2/L$. In theory, this allows us complete freedom over two adhesion parameters, spring stiffness K and range y_c as long as they satisfy the constraint $J = nKy_c^2/L$. Even better, if we also know the range/cutoff y_c, we might assume K is determined by $K = JL/(ny_c^2)$ and thus scales as $1/n$. Surprisingly, we will show that both of these expectations are entirely wrong. For instance, simulations clearly indicate that hysteresis vanishes as we increase n while scaling $K \sim 1/n$ (Fig. S4A).

To understand this, we can rewrite Eq. (S.4), multiplying by n to get total scaled energy loss $n\,\delta e$ (summed over all n bonds) and substituting the invariant J for $K = JL/(ny_c^2)$:

$$n\delta e \sim \frac{L^2}{ny_c}\left(\frac{J}{B}\right)^{1/2}, \tag{S.6}$$

From this, we see that scaling $K \sim 1/n$ while keeping y_c constant results in hysteresis $n\,\delta e$ vanishing as $1/n$. This predicted exponent indeed matches the simulation data (Fig. S4B).

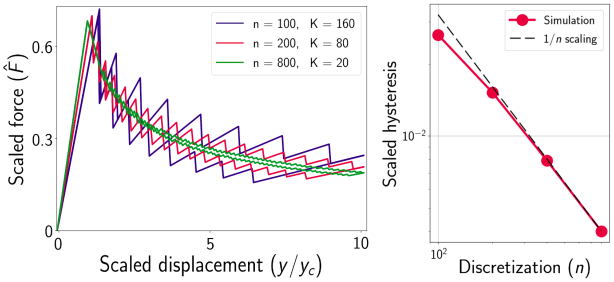

FIG. S4. (A) Scaled force $\hat{F} \equiv F/(By_c/l_H^3)$ versus scaled free end displacement y/y_c for simulations in which adhesion energy per unit length $J = nKy_c^2/L$ is kept constant through scaling $K \sim 1/n$. Parameters: $L = 16\,\mu$m, $B = 22\,pN\,\mu$m^2, $y_0 = 5$ nm, $y_c = 10$ nm. (B) Log-log plot of scaled hysteresis (red) versus the number of adhesive bonds n, which varies from $n = 100$ to $n = 800$. Parameters correspond to those in panel A. Scaled hysteresis is calculated as the area enclosed by the force-displacement curves in panel A. The predicted $1/n$ scaling (black dashed line) agrees very well with simulations for larger n, while deviations at smaller n are explained by discrete size effects.

Equation (S.6) also tells us the proper scaling of adhesion parameters that preserves hysteresis under fine/coarse-graining: since everything else on the right hand side is constant, we must have $ny_c =$ constant, i.e.

$y_c \sim 1/n$, which then implies $K \sim n$ (in order to keep J constant). This scaling is confirmed by simulations (Fig. S5A). Thus, we can write $K = An$ and $y_c = C/n$, where A and C are constants. At first glance, it is tempting to assume that any choice of A and C satisfying the constraint $J = AC^2/L$ is equally valid. In fact, no degeneracy is possible in choosing these constants, as different choices of $C = ny_c$ will change the amount of hysteresis:

$$n\delta e \sim \frac{L^2}{ny_c}\left(\frac{J}{B}\right)^{1/2} = \frac{L^2}{C}\left(\frac{J}{B}\right)^{1/2}. \qquad \text{(S.7)}$$

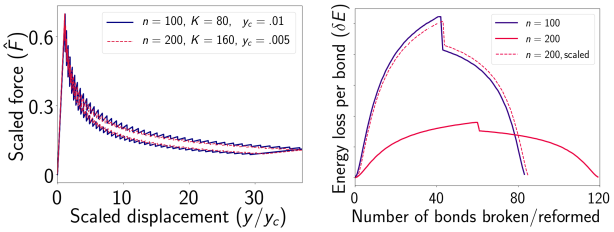

FIG. S5. (A) Scaled force $\hat{F} \equiv F/(By_c/l_H^3)$ versus scaled free end displacement y/y_c for simulations in which adhesion energy per unit length $J = nKy_c^2/L$ is kept constant through scaling $K \sim n$ and $y_c \sim 1/n$. Parameters: $L = 8\,\mu$m, $B = 22\,pN\,\mu\text{m}^2$. (B) Energy loss per bond broken or reformed, δE, versus the cumulative number of bonds broken or reformed for the two simulations in panel A, with $n = 100$ (blue line) and $n = 200$ (solid red line). The two profiles can be made to collapse (signifying equal scaled hysteresis size) by scaling the horizontal axis by a factor $\Delta l/l_H$ and the vertical axis by the bending energy scale E_b^0.

This implies – surprisingly – that there exists a *single* self-consistent way of fine/coarse-graining a system while preserving hysteresis, i.e. a unique choice for the constants A and C. In practice, to find these constants, we can either try to estimate C from Eq. (S.7), where for $n\,\delta e$ we can substitute hysteresis size scaled by a bending energy scale, or we can simply consider C as a parameter which we fit to the data.

The same principles also apply in the more general case in which both filaments are flexible: equation (S.5) suggests the proper scaling of the adhesive parameters K and y_c ($K \sim n^3$ and $y_c \sim 1/n^2$) and indicates that no degeneracy is possible in choosing the constants A and C, where $K = An^3$ and $y_c = C/n^2$. Overall, our results provide a recipe for correctly discretizing a continuous system while preserving hysteresis.

S.4. HYSTERESIS IN GRAPHENE PEELING EXPERIMENTS

To test our theory on real data, we refer to experiments such as those involving peeling adherent microtubules, where we showed we can reproduce the onset and approximate size of hysteresis (Fig. 4, main text). In the limit

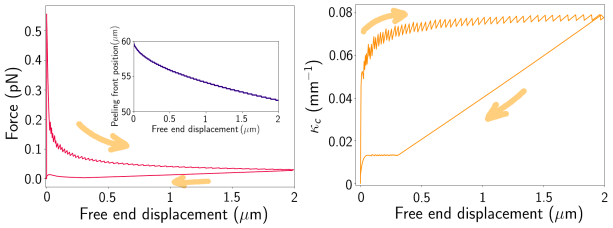

FIG. S6. (A) Force versus displacement for simulating hysteresis in peeling graphene [5]. (Inset): Position of the peeling boundary versus vertical displacement of the free end. (B) Curvature at the peeling boundary κ_c versus displacement of the free end for the same parameter values. Parameters: $L = 60\mu$m, $B = 3$, $K = 1000$, $y_c = 0.0005$, $n = 200$.

of peeling from a flat substrate, we refer to a recent paper reporting substantial hysteresis in peeling a graphene sheet from a flat surface, with the energy required for delamination roughly 100 times larger than the energy recovered when readhered [5]. The graphene sheet has length $L = 60\,\mu$m, bending rigidity $B \approx 3{\times}10^9\,pN{\times}\mu\text{m}^2$, and effective adhesion energy per unit length $J \approx 10^6\,pN$. Using these parameters, and choosing a discretization size $n = 80$, we can find a value of C for which we recover good agreement with the graphene data in the factor of ~ 10 difference between curvature κ_c in the peeling regime compared to that in the healing regime (Fig. S6B). In addition, the peeling front displacement of around 5 μm per μm of vertical displacement (Fig. S6A, inset) is within a factor of two from the value measured in the graphene paper.

Interestingly, hysteresis in the graphene peeling experiments is significantly larger than in our microtubule experiments, a fact which is consistent with the predictions of our theory. To see this, note that equations S.5 and S.6 express scaled hysteresis for the two cases (different geometries) in terms of three length scales: L, $\sqrt{B/J}$, and y_c. Specifically, both equations predict that scaled hysteresis is proportional to length L as well as inversely proportional to the interaction cutoff y_c and to $\sqrt{B/J}$. While $\sqrt{B/J}$ is comparable between the two experiments, the other two length scales are not. The length of the graphene sheet is slightly larger ($L^{\text{gr}} = 60\mu\text{m} > L^{\text{MT}} \sim 10\mu\text{m}$) and, most importantly, the interaction in the graphene experiments is much shorter-range: $y_c^{\text{gr}} \sim 0.1$ nm $\ll y_c^{\text{MT}} \sim 15$ nm. Thus, the short interaction range/cutoff in graphene is responsible for the very high hysteresis observed experimentally.

Physically, we can understand the inverse dependence of hysteresis on y_c by noting that, everything else being constant (i.e. L, B, and J), reducing y_c results in stiffer springs K (since $J = nKy_c^2/L$ is constant). When one of these springs break, it will have a relatively large effect on the stress redistribution which will cause the newly broken bond to "jump" significantly (as in the inset of the schematic in Fig. 1A). We can see how such a jump

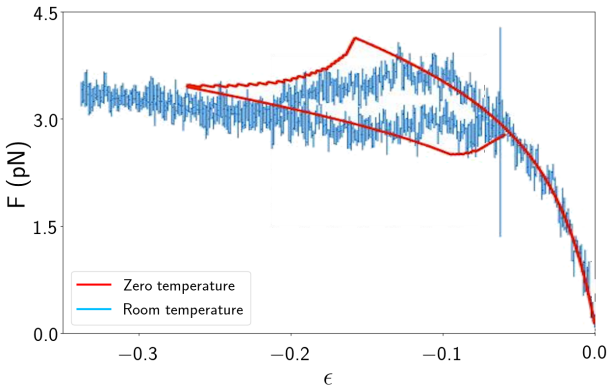

FIG. S7. Simulations of microtubule fraying with (blue) and without (red) thermal fluctuations. Parameters: $L = 8\,\mu$m, $B = 22\,pN\,\mu\text{m}^2$, $K = 500\,pN/\mu$m, $n = 100$, $y_0 = 5\,$nm, $y_c = 10\,$nm, $L_2 = 0.7L$.

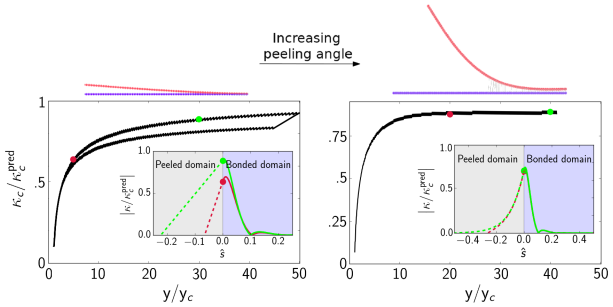

FIG. S8. Top: Peeling angle increases with y/l_H. Bottom: Plots of scaled curvature at the peeling boundary $\kappa_c/\kappa_c^{\text{pred}}$ as a function of scaled end displacement y/y_c for a simulation with low peeling angle (parameters: $L = 16\,\mu$m, $B = 44\,pN\,\mu\text{m}^2$, $K = 40\,pN/\mu$m, $n = 400$, $y_0 = 5\,$nm, $y_c = 10\,$nm) as well as one with a higher peeling angle (same parameters except for $y_0 = 100\,$nm, $y_c = 300\,$nm).

relates to hysteresis by noting that if the direction of the free end displacement is reversed, the newly broken bond will have to travel extra distance (due to the jump) in order to re-enter the interaction range. In contrast, larger y_c means weaker springs, less effect of bond breakage, and thus less of a jump in the position of the broken bond (and consequently, smaller hysteresis).

S.5. THE EFFECT OF THERMAL FLUCTUATIONS ON HYSTERESIS

While experiments were conducted at room temperature, simulations were mainly done in the absence of thermal fluctuations. Intuitively, we expect that thermal fluctuations can cause an earlier onset of peeling as well as healing, resulting in a narrowing of the hysteresis loop [6]. The extent of this narrowing effect depends on the relative strength of thermal fluctuations compared to adhesion energy. For example, the adhesion energy per unit length in the microtubule experiments is $J \approx 25K_BT/\mu$m, suggesting that thermal energy can compete with adhesion on scales of order $1/25\mu$m or smaller. Therefore, for typical values of adhesion encountered in the microtubule experiments, we expect to see a moderate extent of narrowing of the hysteresis curve in the presence of thermal fluctuations. This is indeed what we observe in comparing simulations with and without thermal fluctuations under the same conditions (Fig. S7). In the case of graphene, adhesion is much stronger than in the microtubule experiments, so that thermal fluctuations should have practically no noticeable effect.

S.6. PEELING ANGLE

Intuitively, the peeling angle of the displaced filament is related to the dimensionless ratio of transverse and longitudinal length scales y_c/l_H (Fig. S8). While the peeling angle does not directly influence the response inside the bonded region (Eq. 2 and 3), it does determine how curvature decays outside the bonded region, from κ_c at the peeling boundary to 0 at the free end. In the limit of a low peeling angle α, curvature decays linearly from κ_c to 0 (Fig. S8, left inset); consequently, as the length of the peeled segment increases, so does the size of this linear tail, causing the bending energy to continually increase. On the other hand, for a high peeling angle α, the region of curvature decline in the debonded zone remains fairly constant in size (Fig. S8, left inset), such that bending energy saturates (as in Fig. 1B in the main text).

Denoting the vertical displacement of the free end by y and the length of the peeled filament by s, we have from geometrical arguments:

$$\kappa_c \sim \frac{y}{s^2} = \frac{y_c}{l_H^2}. \tag{S.8}$$

Therefore, the peeling angle $y/s \sim y_c\, s/l_H^2$. The above equation suggests that $s \sim \sqrt{y}$, i.e. the length of the peeled region scales as the square root of the vertical displacement.

S.7. FRAYING INSTABILITY

The microtubule fraying simulations can exhibit a peeling instability under certain parameter values. Typically, peeling occurs incrementally: the optical bead is displaced by a small amount and the system is allowed to relax, which can lead to a single bond breaking. However, under certain conditions we have also observed a runaway effect, such that once the first bond breaks, it leads to a cascade of bond breaking events. That is, rather than incrementally peeling, the filament suddenly peels by a very large amount even though the optical bead was displaced only by a small amount. Video S1 illustrates this phenomenon.

[1] A. Arnold, O. Lenz, S. Kesselheim, R. Weeber, F. Fahrenberger, D. Roehm, P. Košovan, and C. Holm, in *Meshfree Methods for Partial Differential Equations VI* (Springer, 2013) pp. 1–23.
[2] F. Weik, R. Weeber, K. Szuttor, K. Breitsprecher, J. de Graaf, M. Kuron, J. Landsgesell, H. Menke, D. Sean, and C. Holm, The European Physical Journal Special Topics **227**, 1789 (2019).
[3] E. Memet, F. Hilitsk, M. A. Morris, W. J. Schwenger, Z. Dogic, and L. Mahadevan, eLife **7**, e34695 (2018).
[4] R. Thomson, C. Hsieh, and V. Rana, J. Appl. Phys. **42**, 3154 (1971).
[5] M. Z. Miskin, C. Sun, I. Cohen, W. R. Dichtel, and P. L. McEuen, Nano letters **18**, 449 (2017).
[6] K. Kitamura, I. Maksimov, and K. Nishioka, Philosophical magazine letters **75**, 343 (1997).